A Search for $\nu_\mu \to \nu_e$ and $\overline{\nu}_\mu \to \overline{\nu}_e$ Oscillations at NuTeV

S. Avvakumov[8], T. Adams[4], A. Alton[4], L. de Barbaro[5], P. de Barbaro[8], R. H. Bernstein[3], A. Bodek[8], T. Bolton[4], J. Brau[6], D. Buchholz[5], H. Budd[8], L. Bugel[3], J. Conrad[2], R. B. Drucker[6], B. T. Fleming[2], R. Frey[6], J.A. Formaggio[2], J. Goldman[4], M. Goncharov[4], D. A. Harris[8], R. A. Johnson[1], J. H. Kim[2], S. Koutsoliotas[2], M. J. Lamm[3], W. Marsh[3], D. Mason[6], J. McDonald[7], K. S. McFarland[8,3], C. McNulty[2], D. Naples[7], P. Nienaber[3], V. Radescu[7], A. Romosan[2], W. K. Sakumoto[8], H. Schellman[5], M. H. Shaevitz[2], P. Spentzouris[2], E. G. Stern[2], N. Suwonjandee[1], M. Tzanov[7], M. Vakili[1], A. Vaitaitis[2], U. K. Yang[8], J. Yu[3], G. P. Zeller[5], and E. D. Zimmerman[2]

[1] *University of Cincinnati, Cincinnati, OH 45221*
[2] *Columbia University, New York, NY 10027*
[3] *Fermi National Accelerator Laboratory, Batavia, IL 60510*
[4] *Kansas State University, Manhattan, KS 66506*
[5] *Northwestern University, Evanston, IL 60208*
[6] *University of Oregon, Eugene, OR 97403*
[7] *University of Pittsburgh, Pittsburgh, PA 15260*
[8] *University of Rochester, Rochester, NY 14627*

(February 7, 2008)

Limits on $\nu_\mu \to \nu_e$ and $\overline{\nu}_\mu \to \overline{\nu}_e$ oscillations are extracted using the NuTeV detector with sign-selected ν_μ and $\overline{\nu}_\mu$ beams. In $\overline{\nu}_\mu$ mode, for the case of $\sin^2 2\alpha = 1$, $\Delta m^2 > 2.6$ eV^2 is excluded, and for $\Delta m^2 \gg 1000$ eV^2, $\sin^2 2\alpha > 1.1 \times 10^{-3}$. The NuTeV data exclude the high Δm^2 end of $\overline{\nu}_\mu \to \overline{\nu}_e$ oscillations parameters favored by the LSND experiment without the need to assume that the oscillation parameters for ν and $\overline{\nu}$ are the same. We present the most stringent experimental limits for $\nu_\mu(\overline{\nu}_\mu) \to \nu_e(\overline{\nu}_e)$ oscillations in the large Δm^2 region.

PACS numbers: 14.60.Pq, 13.15.+g ; *UR-1640 to be published in Phys. Rev. Lett.*

Experimental evidence for oscillations among the three neutrino generations has been recently reported. For two-generation mixing, the probability that a neutrino created as type ν_1 oscillates to type ν_2 is:

$$P(\nu_1 \to \nu_2) = \sin^2 2\alpha \sin^2\left(\frac{1.27\Delta m^2 L}{E_\nu}\right), \qquad (1)$$

where Δm^2 is the mass squared difference between the mass eigenstates in eV^2, α is the mixing angle, E_ν is the incoming neutrino energy in GeV, and L is the distance between the points of creation and detection in km.

Data from the Super-Kamiokande atmospheric neutrino experiment [1] have been interpreted as evidence for $\nu_\mu \to \nu_\tau$ oscillations with $\sin^2 2\alpha > 0.88$ and $1.6\times10^{-3} < \Delta m^2 < 4 \times 10^{-3}$ eV^2. The LSND experiment has reported [3] a signal consistent with $\bar{\nu}_\mu \to \bar{\nu}_e$ oscillations with $\sin^2 2\alpha \approx 10^{-2}$ and $\Delta m^2 \gtrsim 1$ eV^2 . The solar neutrino experiments, and most recently SNO [2] have reported evidence for oscillations of $\nu_e \to (\nu_\mu, \nu_\tau)$ with $\Delta m^2 < 10^{-3}$eV^2. Within a three-generation mixing scenario and under the assumption that the Δm^2 values for ν and $\overline{\nu}$ are the same, it is not possible to simultaneously accommodate the Super-Kamiokande, LSND, and SNO results. Therefore, experimental searches for oscillations with both ν and $\overline{\nu}$ beams are of interest. In this letter, we report on a search for oscillations in both the $\nu_\mu \to \nu_e$ and $\overline{\nu}_\mu \to \overline{\nu}_e$ channels using a new sign-selected neutrino beam.

High-purity ν and $\overline{\nu}$ beams are provided by the new Sign-Selected Quadrupole Train (SSQT) beamline at the Fermilab Tevatron during the 1996-1997 fixed target run. Hadrons are produced when the 800 GeV primary proton beam interacts in a BeO target located 1436 m upstream of the neutrino detector. Sign-selected secondary particles of specified charge (mean energy of about 250 GeV) are directed in a 221 m beamline towards a 320 m decay region, while oppositely charged (and neutral) mesons are stopped in beam dumps. Two-body decays of the focused pions yield ν_μ ($\overline{\nu}_\mu$) with a mean energy of ≈75 GeV. Two-body decays of the focused kaons yield ν_μ ($\overline{\nu}_\mu$) with a mean energy of ≈200 GeV. Muons are stopped in a 915 m steel/earth shield.

The energy and spatial distributions of ν_μ ($\overline{\nu}_\mu$) CC events in the detector provide a determination of the flux of pions and kaons in the decay channel (used in the determination of the predicted ν_e and $\overline{\nu}_e$ fluxes). For ν_μ running mode, the predicted energy spectra for ν_μ, $\overline{\nu}_\mu$, and (ν_e+$\overline{\nu}_e$) CC events are shown in Figure 1(a). The corresponding spectra for $\overline{\nu}_\mu$ running mode are shown in Figure 1(b). The ν_μ ($\overline{\nu}_\mu$)beam contains a 1.7% (1.6%) ν_e's($\overline{\nu}_e$'s) 93% and 70% of which are produced from $K^\pm \to \pi^0 e^\pm \overset{(-)}{\nu}_e$, for ν and $\overline{\nu}$ modes, respectively. The proton beam is incident on the production target at an angle such that forward neutral kaons do not point at the detector. This greatly reduces the electron neutrino flux from neutral kaon decays (which is more difficult to

model). The error in the predicted electron neutrino flux is reduced from 4.1% (in CCFR [4]) to 1.4% (NuTeV).

The NuTeV detector [5] is an upgrade of the CCFR detector [6]. It consists of an 18 m long, 690 ton total absorption target-calorimeter with a mean density of 4.2 g/cm^3. Muon energy is measured by a 10 m long iron toroidal spectrometer. The target consists of 168 steel plates, each 3 m × 3 m × 5.15 cm, instrumented with liquid scintillation counters placed every two steel plates and drift chambers every four plates. The separation between consecutive scintillation counters corresponds to six radiation lengths. The energy resolution of the target calorimeter is $\Delta E_h/E_h \approx 0.85/\sqrt{E_h}(\mathrm{GeV})$, and $\Delta E_e/E_e \approx 0.50/\sqrt{E_e}(\mathrm{GeV})$ for hadrons and electrons, respectively. The muon momentum resolution is $\Delta p_\mu/p_\mu = 0.11$. The NuTeV detector is calibrated continuously every accelerator cycle (once a minute) with beams of electrons, muons, and hadrons during the slow spill part of the cycle.

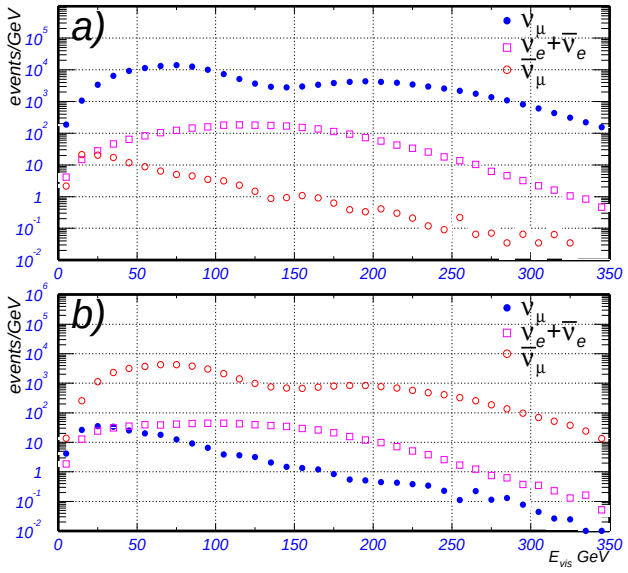

FIG. 1. (a) The predicted visible energy spectra for ν_μ, $\overline{\nu}_\mu$, and (ν_e,$\overline{\nu}_e$) CC-events in ν_μ running mode. (b) The corresponding spectra for $\overline{\nu}_\mu$ running mode. The predictions come from a beam simulation tuned to agree with the observed number of ν_μ or $\overline{\nu}_\mu$ CC events in each running mode.

While the neutrinos arrived in gates a few *msec* wide, the calibration beam arrived in a different gate 20 *sec* long, followed by an off-spill cosmic ray gate for background measurement. These continuous test beam calibrations yield a reduction in the hadron energy scale error from 1% (in CCFR [6]) to 0.43% (in NuTeV [5]).

The event sample used in this analysis is similar to that used in the recent precise NuTeV measurement of the electroweak mixing angle [7] with additional fiducial cuts, and $E_{\mathrm{cal}} > 30$ GeV. The data sample consists of 1.5 x 10^6 ν events and 0.35 x 10^6 $\overline{\nu}$ events with a mean visible energy in the calorimeter (E_{cal}) of 74 GeV and 56 GeV, respectively. The observed neutrino events are separated into CC and NC candidates. Both CC and NC interactions initiate a cascade of hadrons in the target that is registered in both the scintillation counters and drift chambers. Muon neutrino CC events are distinguished by the presence of a final state muon, which typically penetrates well beyond the hadronic shower and deposits energy in a large number of consecutive scintillation counters. NC events usually have no final state muon and deposit energy over a range of counters typical of a hadronic shower (about ten counters ≈ 1 m of steel). For each event, the length (L) is defined as the number of scintillation counters between the interaction vertex and the last counter consistent with at least single muon energy deposition. A pure sample of $\nu_\mu N \to \mu^- X$ ν_μ charged current events is obtained from a 'long' sample with $L \geq 29$ for ν running mode ($L \geq 28$ for $\overline{\nu}$). The "short' event sample consists of events with $L \leq 28$ for ν running mode ($L \leq 27$ for $\overline{\nu}$). Events with a 'short' length are primarily NC induced and originate from:

1. $\nu_{\mu,e} N \to \nu_{\mu,e} X$; $\nu_{\mu,e}$ NC events; (≈ 65%);
2. $\nu_\mu N \to \mu^- X$; ν_μ short CC events with muons which range out or exit the side of the calorimeter (25% for ν, 15% for $\overline{\nu}$);
3. $\nu_e N \to e X$ ν_e CC events (10% for ν, 15% for $\overline{\nu}$);
4. $\mu N \to \mu X$; steep cosmic ray interactions (2% for ν and 9% for $\overline{\nu}$).

The electron produced in a ν_e CC event (source 3) deposits energy in a few counters immediately downstream of the interaction vertex; this changes the longitudinal energy deposition profile of the shower. The energy profile is characterized by the ratio of the sum of the energy deposited in the first three scintillation counters to the total visible energy in the calorimeter E_{cal}:

$$\eta_3 \equiv \frac{E_1 + E_2 + E_3}{E_{\mathrm{cal}}}, \qquad (2)$$

where E_i is the energy deposited in the i^{th} scintillation counter downstream of the interaction vertex, and E_{cal} is the sum of the energy in the 20 scintillation counters downstream (plus 1 upstream) of the vertex. We similarly define η_2 to be the ratio of the sum of the energy deposited in the first two scintillation counters to E_{cal}.

Although the electromagnetic shower component is typically much shorter than a hadron shower, NC and ν_e CC interactions cannot be separated on an event-by-event basis. However, the difference in the shower profiles can be used to perform a statistical extraction of the number of ν_e CC events in the "'short' sample using the η_3 distribution.

We first assume that (for the same final state hadron energy) hadron showers produced in NC and CC interactions are the same. Any difference in the η_3 (or η_2)

distributions of 'long' and 'short' events is attributed to the presence of ν_e CC interactions in the 'short' sample. To compare directly the 'long' and 'short' events, a muon track from the data is added to the 'short' events to compensate for the absence of a muon in NC events. The fraction f of ν_μ CC (source 2) events with a low energy muon contained in the 'short' sample which now have two muon tracks is estimated from a detailed Monte Carlo of the experiment. A simulated sample of such events is obtained by choosing 'long' events with the appropriate energy distribution from the data to which a second short muon track is added in software. The length of the short track and the angular distribution are obtained from a Monte Carlo of ν_μ CC events.

A sample of ν_e CC interactions in our detector is simulated by adding a GEANT [10] generated electromagnetic shower of the appropriate electron energy to the calorimetry counter energies in events in the 'long' data sample. There is good agreement between the GEANT simulation of electrons and the test beam data. The energy distribution of the electron neutrinos and the fractional energy transfer y (in each event) are generated using a detailed Monte Carlo simulation of the experiment. The CC cross section model is tuned to agree with the measured CCFR differential cross sections [8] for ν_μ events. Since the hadron showers in the 'long' sample already have a muon track, this sample ($\nu_e CC + \mu$) can be compared directly with the 'short' and 'long' samples.

The 'long' and 'short' η_3 distributions are further corrected by subtracting the contamination due to cosmic ray events. The cosmic ray component (source 4), which is only important for very low energy bins, is well measured using the off-spill cosmic ray data. Additionally, the η_3 distribution of short ν_μ CC events (source 2), normalized to the predicted fraction f, is subtracted from the 'short' event sample.

To extract the number of ν_e CC events in each $E_{\rm cal}$ bin, we fit the corrected shape of the observed η_3 distribution for the 'short' sample to a combination of ν_μ CC and ν_e CC distributions with appropriate muon additions:

$$[\text{short} + \mu] = \alpha\,[\nu_\mu \text{CC}] + \beta\,[\nu_\text{e}\text{CC} + \mu]. \qquad (3)$$

At this point we improve [9] over the previous CCFR analysis [4] by correcting for additional effects. First, the hadron shower in CC events also includes the contribution of photons that are radiated from the muon during the CC scattering process. These photons are not present in hadron showers of NC events. A correction is applied by using the PYTHIA Monte Carlo [11] to generate the spectrum of photons radiated by the muon in CC events. The parameters in PYTHIA that govern the emission of photons are tuned to yield agreement with the radiative corrections formalism of deRujula [12]. Second, the procedures of adding a muon in software to the 'short' sample (to model a 'long' event) and of modeling electron neutrino events by adding GEANT-generated electromagnetic showers to hadron showers from 'long' events are corrected for imperfect modeling using a full LEPTO/GEANT/GHEISHA simulation of the experiment and analysis procedures. In the GEANT simulation of neutrino events, the Lund Model is used to generate the initial particle composition of hadron showers. The entire experimental procedure is simulated with the beam Monte Carlo (ν_e,$\overline{\nu}_e$) flux as input. Modeling corrections are extracted for each $E_{\rm cal}$ bin from the small difference between the extracted (ν_e,$\overline{\nu}_e$) flux using simulated data and the flux extracted using perfect modeling in the Monte Carlo.

The absolute flux of ν_e's is taken as the average of the results from analyses done using the η_3 and η_2 variables (the statistical error from the η_3 analysis is used) . An additional systematic error (2.3% in neutrino mode and 0.6% in antineutrino mode) is included to account for this difference. This systematic error for antineutrinos is smaller because the final state positron carries a much larger fraction of the energy in $\overline{\nu}_e$ CC events.

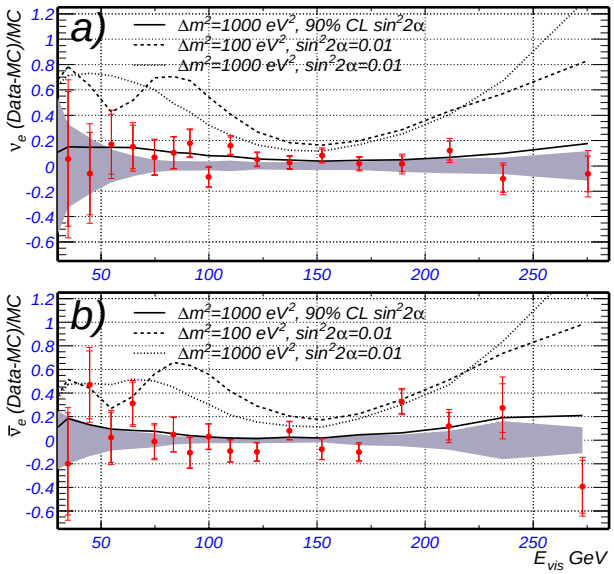

FIG. 2. The ratio of the detected over predicted numbers of (ν_e,$\overline{\nu}_e$) events versus visible energy minus 1. The curves correspond to the predictions for oscillations with $\sin^2 2\alpha = 0.01$, and Δm^2 of 100 and 1000 eV^2. The solid line is the 90% confidence upper limit for Δm^2=1000 eV^2. The shaded area corresponds to the systematic error band.

For the oscillation search we measure the absolute flux of ν_e's at the detector and compare it to the flux predicted by a detailed beamline simulation [7,9]. In order to extract limits on oscillations, the data are fitted by forming a χ^2 which incorporates the Monte Carlo generated effect of oscillations and terms with coefficients accounting for systematic uncertainties. A best fit $\sin^2 2\alpha$ is determined for each Δm^2 by minimizing the χ^2 as a function of $\sin^2 2\alpha$ and these systematic coefficients. Fig-

ure 2 show the ratios of the measured rate of (ν_e,$\overline{\nu}_e$) CC events to the Monte Carlo predictions minus 1. The inner errors are the statistical errors. In order to show the magnitude of the systematic errors, the outer errors include all systematic errors added in quadrature (in the analysis all correlations are taken into account). The shaded area in the figure corresponds to the systematic error band from uncertainties in the predicted electron flux (primarily from the error in the $K^{\pm}$ branching ratio) and uncertainties in the measured flux at the detector (primarily from the η_3,η_2 difference, and the 2% error in the electron energy scale). The curves correspond to the predictions for oscillations with $\sin^2 2\alpha = 0.01$, and Δm^2 of 100 and 1000 eV^2.

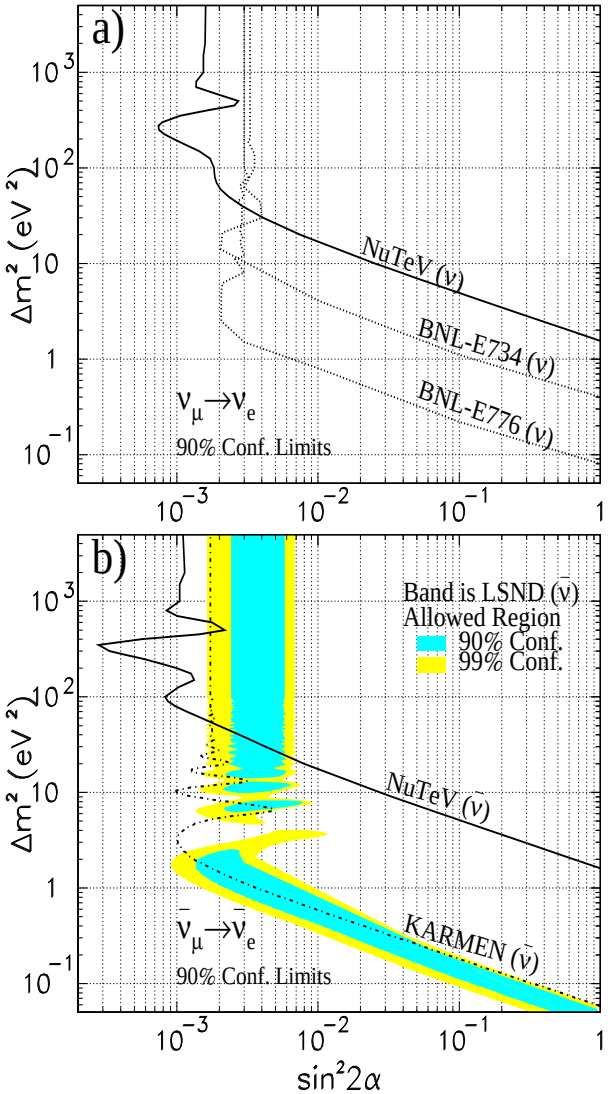

FIG. 3. (a) Excluded region of $\sin^2 2\alpha$ and Δm^2 for $\nu_\mu \to \nu_e$ oscillations from the NuTeV analysis at 90% confidence is the area to the right of the dark, solid curve. (b) NuTeV limits for $\overline{\nu}_\mu \to \overline{\nu}_e$.

At all Δm^2, the data are consistent with no observed $\nu_\mu \to \nu_e$ oscillations (i.e. the best fit values of $\sin^2 2\alpha$ are within one standard deviation of zero). The frequentist approach [13] is used to set a 90% confidence upper limit for each Δm^2. The limit in $\sin^2 2\alpha$ corresponds to a shift of 1.64 units in χ^2 from the minimum (including all systematic errors). The 90% confidence upper limit is shown in Fig. 3(a) for $\nu_\mu \to \nu_e$. Also shown are limits from BNL-E734 [14] and BNL-E776 [15]. For $\sin^2 2\alpha = 1$, $\Delta m^2 > 2.4$ eV^2 is excluded, and for $\Delta m^2 \gg 1000$ eV^2, $\sin^2 2\alpha > 1.6 \times 10^{-3}$ (the best fit is at 1000 eV^2 is $\sin^2 2\alpha = (0.4 \pm 0.9 \times 10^{-3})$. In the large Δm^2 region, NuTeV provides improved limits for $\nu_\mu \to \nu_e$ oscillations.

Similarly, the limit for $\overline{\nu}_\mu \to \overline{\nu}_e$ is shown Fig. 3(b). Also shown are the LSND [3] results and limits from KARMEN [16]. For the case of $\sin^2 2\alpha = 1$, $\Delta m^2 > 2.6$ eV^2 is excluded, and for $\Delta m^2 \gg 1000$ eV^2, $\sin^2 2\alpha > 1.1 \times 10^{-3}$ (the best fit is at 1000 eV^2 is $\sin^2 2\alpha = (-0.3 \pm 1.1 \times 10^{-3})$. In the $\overline{\nu}_\mu$ mode, our results exclude the high Δm^2 end of $\overline{\nu}_\mu \to \overline{\nu}_e$ oscillations parameters favored by the LSND experiment, without the need to assume that the oscillation parameters for ν and $\overline{\nu}$ are the same. These are the most stringent experimental limits [16] for $\nu_\mu(\overline{\nu}_\mu) \to \nu_e(\overline{\nu}_e)$ oscillations in the large Δm^2 region.

This work was supported by the U.S. Department of Energy, the National Science Foundation, and the Alfred P. Sloan foundation.

[1] T. Toshito, hep-ex/0105023; S. Fukuda *et al.* , Phys. Rev. Lett. **85**, 3999 (2000).
[2] Q. R. Ahmad *et al.* , Phys. Rev. Lett. **87**, 071301 (2001).
[3] A. Aguilar *et al.*, Phys. Rev. **D64**, 112007 (2001); plot for $\overline{\nu}_\mu \to \overline{\nu}_e$ provided by Jeoff Mills.
[4] A. Romosan *et al.*, Phys. Rev. Lett. **78**, 2912 (1997).
[5] D. A. Harris, J. Yu, *et al.*, Nucl. Instrum. Methods, **A447**, 377 (2000).
[6] W. K. Sakumoto *et al.*, Nucl. Instrum. Methods, **A294**, 179 (1990).
[7] G. P. Zeller *et al.*, Phys. Rev. Lett. **88**, 091802 (2002).
[8] U. K. Yang *et al.*, Phys. Rev. Lett. **87**, 251802 (2001). U. K. Yang, PhD thesis, Univ. of Rochester, 2001(UR-1583),www.pas.rochester.edu/yigal/bodek/yangthesis.ps.
[9] S. Avvakumov, PhD thesis, Univ. of Rochester, 2001. (UR-1641,www.pas.rochester.edu/ avva/thesis.ps).
[10] GEANT, detector description and simulation tool, CERN Program Library Long Writeup W5013.
[11] T. Sjöstrand, Comput. Phys. Commun. **82**, 74 (1994).
[12] A. De Rujula *et al.*, Nucl. Phys. **B154**, 394 (1979).
[13] Particle Data Group, Phys. Rev. **D54**, 164 (1996).
[14] L. A. Ahrens *et al.*, Phys. Rev. **D36**, 702 (1987).
[15] L. Borodovsky *et al.*, Phys. Rev. Lett. **68**, 274 (1992).
[16] B. Armbruster *et al.* hep-ex/0203021.